Poly-2-methyl-2-oxazoline–modified bioprosthetic heart valve leaflets have enhanced biocompatibility and resist structural degeneration

Andrey Zakharchenko[a], Yingfei Xue[b], Samuel Keeney[a], Christopher A. Rock[a], Ivan S. Alferiev[a], Stanley J. Stachelek[a], Hajime Takano[c], Tina Thomas[a], Chandrasekaran Nagaswami[d], Abba M. Krieger[e], Michael Chorny[a], Giovanni Ferrari[b], and Robert J. Levy[a,1]

[a]Pediatric Heart Valve Center, Division of Cardiology, Department of Pediatrics, The Children's Hospital of Philadelphia, Philadelphia, PA 19104; [b]Department of Surgery and Biomedical Engineering, Columbia University, New York, NY, 10032; [c]Division of Neurology, Department of Pediatrics, The Children's Hospital of Philadelphia, Philadelphia, PA 19104; [d]Department of Cell and Developmental Biology, University of Pennsylvania School of Medicine, Philadelphia, PA 19104; and [e]Department of Statistics, The Wharton School, University of Pennsylvania, Philadelphia, PA, 19104

Edited by Robert Langer, Chemical Engineering, Massachusetts Institute of Technology, Cambridge, MA; received November 22, 2021; accepted January 4, 2022

Bioprosthetic heart valves (BHV) fabricated from glutaraldehyde-fixed heterograft tissue, such as bovine pericardium (BP), are widely used for treating heart valve disease, a group of disorders that affects millions. Structural valve degeneration (SVD) of BHV due to both calcification and the accumulation of advanced glycation end products (AGE) with associated serum proteins limits durability. We hypothesized that BP modified with poly-2-methyl-2-oxazoline (POZ) to inhibit protein entry would demonstrate reduced accumulation of AGE and serum proteins, mitigating SVD. In vitro studies of POZ-modified BP demonstrated reduced accumulation of serum albumin and AGE. BP-POZ in vitro maintained collagen microarchitecture per two-photon microscopy despite AGE incubation, and in cell culture studies was associated with no change in tumor necrosis factor-α after exposure to AGE and activated macrophages. Comparing POZ and polyethylene glycol (PEG)–modified BP in vitro, BP-POZ was minimally affected by oxidative conditions, whereas BP-PEG was susceptible to oxidative deterioration. In juvenile rat subdermal implants, BP-POZ demonstrated reduced AGE formation and serum albumin infiltration, while calcification was not inhibited. However, BP-POZ rat subdermal implants with ethanol pretreatment demonstrated inhibition of both AGE accumulation and calcification. Ex vivo laminar flow studies with human blood demonstrated BP-POZ enhanced thromboresistance with reduced white blood cell accumulation. We conclude that SVD associated with AGE and serum protein accumulation can be mitigated through POZ functionalization that both enhances biocompatibility and facilitates ethanol pretreatment inhibition of BP calcification.

advanced glycation end products | calcification | thromboresistance | inflammation

Heart valve disease is highly prevalent, affecting millions worldwide, and most commonly involves the mitral or aortic valves (1). Since there is no effective medical therapy, severe, symptomatic disease is treated by cardiac surgery or catheter intervention, often involving implantation of either bioprosthetic or mechanical valve prostheses. Bioprosthetic heart valves (BHV) fabricated from glutaraldehyde-fixed heterografts, such as bovine pericardium (BP), demonstrate many advantages over mechanical valves including reduced thrombogenicity and adaptability to transcatheter deployment (2, 3); the material and mechanical properties of BHV have thus become of increasing scientific interest (4). Despite these benefits, BHV longevity is limited by poor durability due to structural valve degeneration (SVD) that often involves calcification, eventually leading to leaflet dysfunction and clinical failure (5). Our group recently demonstrated that SVD is also due to the accumulation of both advanced glycation end products (AGE) and AGE-modified serum proteins; this was observed in a clinical series of 45 SVD BHV explants, all explants demonstrating AGE-serum protein accumulation. Nevertheless, BHV use is rapidly increasing because of the suitability of heterograft valves for transcatheter delivery, an approach that has numerous advantages over open heart surgery (6). However, BHV implanted with transcatheter delivery systems utilize the same heterograft technology as surgically implanted prostheses, and thus are similarly at risk for SVD limiting durability and increasing risks for reoperation.

Attempts to develop chemical strategies to reduce calcification of BP materials have demonstrated limited success (7). Furthermore, a significant proportion of observed SVD cases (estimated at 25 to 30%) have been shown to be associated with minimal or no calcification (8, 9). AGE and serum proteins, as mentioned above, have only recently been recognized as contributing to SVD. However, prior to the present studies, there have been no investigations of strategies to address AGE-serum protein mechanisms that contribute to SVD. The impact of AGE and related serum protein accumulation by BHV on

Significance

Heart valve disease affects millions, and since there is no effective medical therapy, surgical repair when possible—or more commonly, replacement—are the only treatments available. Bioprosthetic heart valves (BHV), the most frequently used valve replacements, are composed of heterograft tissue, typically fixed in glutaraldehyde, and prepared for human use either as surgically implantable devices or for transcatheter delivery. Protein-glycation limits the durability of BHV, contributing to device failure, often requiring reoperation after only a decade or less of functionality. This problem is addressed by modifying BHV leaflets with poly-2-methyl-2-oxazoline, effectively mitigating glycation and serum protein infiltration and enhancing biocompatibility.

Author contributions: A.Z., Y.X., S.J.S., M.C., G.F., and R.J.L. designed research; A.Z., Y.X., S.K., C.A.R., I.S.A., S.J.S., H.T., T.T., C.N., M.C., and R.J.L. performed research; I.S.A. contributed new reagents/analytic tools; A.Z., Y.X., S.K., C.A.R., S.J.S., H.T., T.T., C.N., A.M.K., M.C., and R.J.L. analyzed data; and A.Z., Y.X., I.S.A., S.J.S., M.C., G.F., and R.J.L. wrote the paper.

The authors declare no competing interest.

This article is a PNAS Direct Submission.

[1]To whom correspondence may be addressed. Email: levyr@email.chop.edu.

This article contains supporting information online at http://www.pnas.org/lookup/suppl/doi:10.1073/pnas.2120694119/-/DCSupplemental.

Published February 7, 2022.

SVD is of importance based on a number of factors. In our series of BHV clinical explants with SVD, the AGE cross-link, glucosepane, was observed to be present per immunohistochemistry (IHC) in each of 45 human explants; increased cross-linking due to glucosepane contributes to leaflet stiffening and progression of SVD (10). In addition, proinflammatory AGE-ligands, such as carboxymethyl lysine (CML) that interact with the white blood cell (WBC) receptor for AGE, known as RAGE, were present per immunostaining in each of these BHV clinical explants (10). These recent discoveries provide the rationale for investigating strategies to limit AGE-serum protein uptake by BHV leaflets.

We chose to investigate modifying BHV leaflet material with poly-2-methyl-2-oxazoline (POZ), based on the following considerations. Polyoxazolines, such as POZ, are a novel class of polymers that have been of primary interest for pharmaceuticals (11); our studies investigate POZ for BHV use. POZ has some structural and functional similarities to polyethylene glycol (PEG) (12, 13). However, PEG modification of BHV leaflets resulted in complement activation and IgG adsorption after exposure to human blood (14). Furthermore, PEG, unlike POZ, is susceptible to oxidation, causing a loss of protective functionality (15, 16). Additionally, as many as 70% of the general population have anti-PEG antibodies as a result of exposure to PEG as a pharmaceutical additive; this creates a risk for an immune response triggered by a PEG-modified implant (17).

The present study evaluated the hypothesis that BHV leaflets covalently functionalized with POZ would demonstrate diminished serum protein accumulation and AGE formation, thereby mitigating the AGE-related inflammatory response and stabilizing hydrodynamic performance by reducing accumulation of AGE-modified serum proteins. We also sought to investigate the blood material interactions of BP-POZ. To investigate BP modified with covalently linked POZ to prevent AGE-driven SVD of BP, we designed and carried out a series of experiments aiming 1) to study in vitro BP-POZ effectiveness at blocking AGE formation and uptake of serum albumin, as a model serum protein; 2) to explore the effects of BP-POZ on limiting the production of proinflammatory cytokines and maintenance of collagen structural integrity after exposure to accelerated glycation conditions in vitro and monocyte-derived macrophages; 3) to compare the stability of the BP-POZ and BP-PEG on AGE-serum protein pathophysiology, upon exposure to an oxidant, hydrogen peroxide (H_2O_2); 4) to investigate in vivo BP-POZ compared to BP with respect to AGE formation, sera protein infiltration, and calcification using an established juvenile rat subdermal implant model, comparing BP-POZ modification with and without ethanol pretreatment to inhibit calcification; and 5) to examine the effects of BP-POZ modification on blood material interactions.

Results

The rationale for these studies (Fig. 1) is based on the fact that although BHV failure is frequently associated with calcification, recent evidence demonstrated that noncalcific failure mechanisms play an important role in SVD (9, 10, 18). Specifically, serum proteins infiltration and AGE formation result in deterioration of the mechanical properties of BP and related collagen fiber disruption (19) (Fig. 1).

Furthermore, the inflammatory processes driven by accumulation of host WBCs and their activation due to RAGE signaling results in reactive oxygen species that can damage the BHV extracellular matrix and results in accelerated valve failure (20). Thus, the objective of these experimental studies was to investigate the effects of modifying BP with POZ on AGE and serum protein SVD mechanisms, blood material interactions, and inflammatory events.

POZ Modification of BP Tissue. For POZ modification of BP tissue (Fig. 2 and *SI Appendix*, Fig. S1), glutaraldehyde-fixed BP tissue samples were reacted with POZ-primary amino groups via a carbodiimide-driven reaction resulting in an amide bond formation (Fig. 2*A*). The amount of covalently bound polymer was quantified fluorimetrically using POZ labeled with a custom synthesized fluorescent probe (F-POZ) (*SI Appendix*, *Supplementary Methods S1* and Fig. S1) admixed with unlabeled polymer (Fig. 2*A*) (fluorescein derivative). To determine the reaction kinetics between POZ and BP, F-POZ was reacted with BP for 24 h in the presence of 1-Ethyl-3-(3-dimethylaminopropyl) carbodiimide (EDC) and *N*-hydroxysuccinimide (NHS), and the amount of bound F-POZ was monitored throughout the reaction (Fig. 2*B*). The reaction was biphasic, proceeding rapidly in the first 3 h, then slowing down, ending with 20 ± 2 μg POZ per gram tissue after 24 h. Fluorescent intensity of F-POZ–modified tissues was unchanged after 30-d incubation at physiological conditions (pH 7.4, 37 °C) in the dark (Fig. 2*C*). This indicated that F-POZ fully penetrates BP collagen fibers in the presence of EDC-NHC, resulting in a stable uniform layer throughout the tissue. Fluorescent microscopy analysis of BP tissue sections revealed negligible green autofluorescence (λex/λem = 490 nm/515 nm) (Fig. 2 *D*, *a*). Tissue incubation in F-POZ followed by addition of EDC-NHS resulted in an intense green fluorescence throughout the tissue (Fig. 2 *D*, *c*), while incubation in F-POZ or EDC/NHS alone did not result in a significant change in fluorescent intensity (Fig. 2 *D* and *E*). BP samples were analyzed with differential scanning calorimetry (DSC), as an index of cross-linking, that showed a small but significant increase in shrink temperature in BP after EDC treatment ($P < 0.005$) and POZ modification ($P < 0.001$) (Fig. 2*F*).

BP-POZ Inhibits Serum Albumin Uptake and AGE Formation by BP Tissue and BP in Trileaflet BHV In Vitro. We next examined accumulation of serum proteins and AGE in BP-POZ compared to unmodified BP. BP samples (unmodified or BP-POZ) were incubated in bovine serum albumin (BSA), a model serum protein that is susceptible to glycation and accumulation in BHV leaflets. BSA uptake was quantified by the change in tissue dry weight over 28 d (Fig. 3*A*). Incubation of control BP samples in BSA resulted in a gradual increase of the mass, which could be detected at 24 h and plateaued at 3.5% after 7 d. By contrast, POZ functionalization inhibited BSA uptake, with no change in tissue dry weight during the first 7 d and a small loss of weight between days 7 and 28. Immunostaining for BSA following 28 d of exposure demonstrated that unmodified BP accumulated BSA uniformly throughout the tissue (Fig. 3 *B*, *b*).

In contrast, BP-POZ samples did not accumulate BSA per immunostaining (Fig. 3 *B*, *c*) and stained similarly to unexposed controls (Fig. 3 *B*, *a*), indicating that POZ functionalization of BP can effectively mitigate the uptake of high molecular weight serum proteins.

The oxidative resistance of POZ compared to PEG was tested by exposure of BP-POZ or BP-PEG to oxidative conditions using H_2O_2. Coincubation of BP with BSA and glyoxal (GLX+BSA) was used as an established glycation model that results in the formation of CML. The extent of glycation was evaluated by IHC for CML (Fig. 3*C*) (21, 22). The oxidation-resistant properties of POZ were compared to PEG by exposure to mild oxidative conditions using BP-POZ, BP-PEG, and BP samples that were exposed for 7 d to H_2O_2 followed by 7 d of GLX+BSA coincubation. BP incubation in PBS, studied as a control comparison, resulted in negative IHC staining for CML (Fig. 3*C*, unmodified), whereas GLX coincubation with BSA caused markedly more intense staining compared to PBS control (Fig. 3*C*, GLX+BSA). Staining intensity for CML was not affected by H_2O_2. However, H_2O_2-exposed PEG-modified samples exhibited a marked increase in CML staining (Fig. 3*C*,

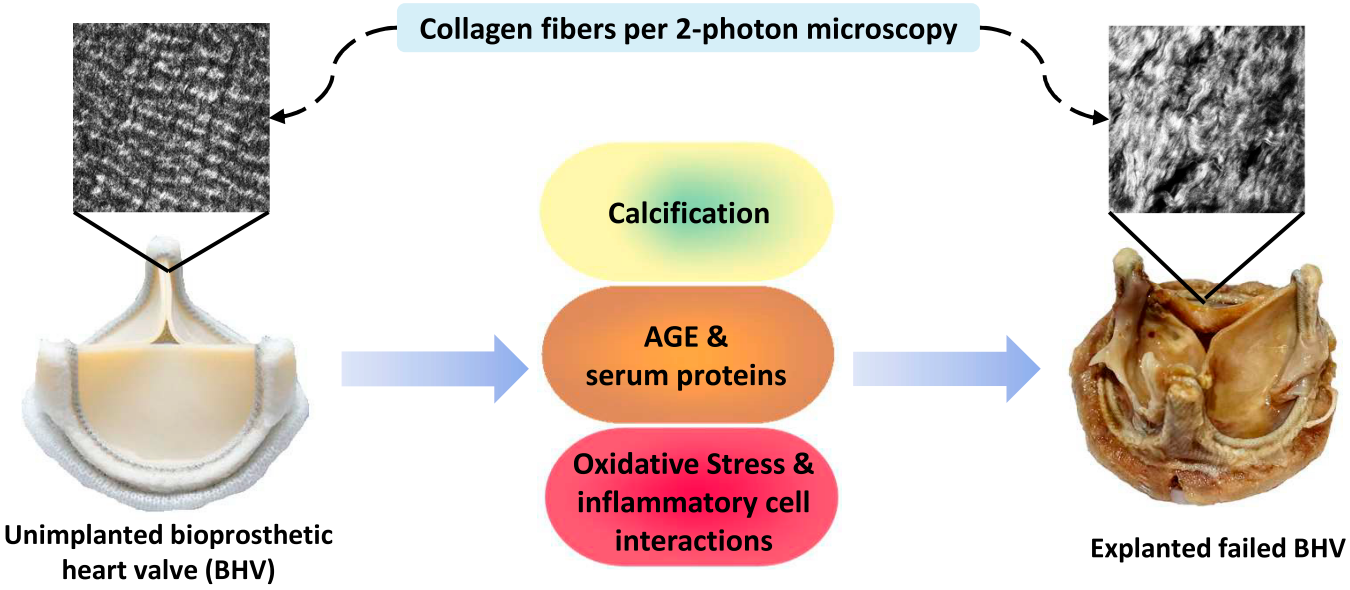

Fig. 1. Mechanisms of BHV failure due to structural degeneration. Calcification and serum proteins infiltration, along with AGE formation and inflammatory-related oxidative stress, result in a deterioration of collagen structure and ultimately device failure, as evident from comparing second harmonic generation confocal micrographs (*Top* images, magnification 40×).

PEG GLX + BSA). Remarkably, the protective effect mediated by POZ resulted in mitigation of CML staining and was unaltered by the exposure to H_2O_2 (Fig. 3*C*, POZ GLX + BSA). Quantification of relative staining intensity using image analysis (*SI Appendix*, *Supplementary Methods S1*) revealed a two fold increase in PEG-modified samples after H_2O_2 exposure, indicating PEG degradation (Fig. 3*D*). On the other hand, POZ-modified samples demonstrated negative IHC staining with minimal change in staining intensity.

To explore the effects of POZ modification on BHV hydrodynamics, five clinical grade trileaflet bioprosthetic valves with BP leaflets were studied, comparing POZ modified to unmodified BHV (*SI Appendix*, *Supplementary Methods S1*, Fig. S4, and Tables S1–S5). These experiments assessed aortic valve hydrodynamics, using an aortic valve pulse duplicator system (*SI Appendix*, *Supplementary Methods S1*), both at baseline and following GLX-HSA incubations over a 35-d time course (*SI Appendix*, *Supplementary Methods S1*, *Supplementary Results S1*, Fig. S4, and Tables S1–S5). Baseline testing of trileaflet BHV before and after POZ modification (*SI Appendix*, Tables S2 and S5) demonstrated that POZ modification does not significantly alter the initial hydrodynamics. The results also demonstrated minimal changes in baseline hydrodynamic properties comparing POZ to non-POZ BHV (*SI Appendix*, *Supplementary Results S1*, Fig. S4, and Tables S1–S5), and small, but statistically significant changes in endpoints including pressure gradient, effective orifice area, and peak ejection velocity, indicating mitigation of GLX-HSA effects on hydrodynamics with BP leaflets modified with POZ (*SI Appendix*, Fig. S4).

BP-POZ Demonstrates Stable Collagen Structure and Reduced Glycation-Associated Inflammatory Cytokine Production in Macrophage Cell Cultures. BP collagen microstructure was examined by second-harmonic imaging (SHG) microscopy before (Fig. 4*A*) and after (Fig. 4*B*) exposure to THP-1 cells (monocyte-derived macrophages), and the crimp period of collagen fibers per SHG was quantified by pixel measurement of distance between crimp bands, as described previously (19). Based on the SHG images, the samples had consistent, well-organized collagen architecture prior to macrophage exposure (Fig. 4 *A*, *a–d*). Incubation of the samples with macrophages resulted in the disruption of the collagen structure in glucose glycated BSA (GLU-BSA), GLX, and GLX+BSA samples (Fig. 4 *B*, *b–d*). Disruption of the collagen alignment was most noticeable in GLX+BSA samples (Fig. 4 *B*, *d*). All BP-POZ samples demonstrated consistent fiber alignment and a distinctive crimp morphology before (Fig. 4 *A*, *e–h*) and after (Fig. 4 *B*, *e–h*) exposure to THP-1. Analysis of the crimp period after exposure to cells revealed no significant changes for BP-POZ samples incubated with PBS (Fig. 4*C*), indicating that POZ attachment did not alter the collagen microarchitecture. Furthermore, BP-POZ did not demonstrate any structural changes following exposure to glycation conditions in the GLU-BSA (Fig. 4*C*) [POZ (+) cells] -treated samples. However, in the absence of POZ, incubation of BP with GLU-BSA (Fig. 4*C*) [unmodified (+) cells] followed by exposure to THP-1 cells resulted in a significant increase of the crimp period; this change was fully prevented by BP-POZ (Fig. 4*C*) [POZ (+) cells]. Interestingly, there was a significant crimp change in all GLX-incubated samples (Fig. 4*C*, GLX). Whereas BP-POZ exposed to GLX+BSA resulted in a significant change in crimp period; the mean value decreased and was similar to GLX (Fig. 4*C*, GLX-BSA vs. GLX). These observations indicate that BP-POZ demonstrated resistance to BSA-associated glycation, but did not restrict diffusion of small molecules, such as GLX.

The effects of BP-POZ and BSA-glycation exposure on the inflammatory state of activated human derived THP-1 macrophages were studied with BP-POZ and BP samples. Phorbol 12-myristate 13-acetate (PMA) -activated THP-1 were seeded on the various BP samples for 24 h, then incubated in fresh media for 48 h and the cell culture media was analyzed to determine the concentration of the inflammatory cytokine tumor necrosis factor-α (TNF-α) (Fig. 4*D*). BP or BP-POZ were incubated for 7 d in either PBS, glucose-BSA (GLU-BSA), GLX, or GLX+BSA; following this, the BP samples were used as substrates for activated macrophages. There was no significant effect of BP-POZ modification on the number of adherent cells. Furthermore, THP-1 exposure to BP-POZ in PBS induced a significant reduction ($P < 0.05$) in TNF-α production compared to unmodified BP, indicating the biocompatible and nontoxic nature of POZ (Fig. 4*D*, PBS). Preincubation of BP with GLU-BSA followed by THP-1 macrophage exposure

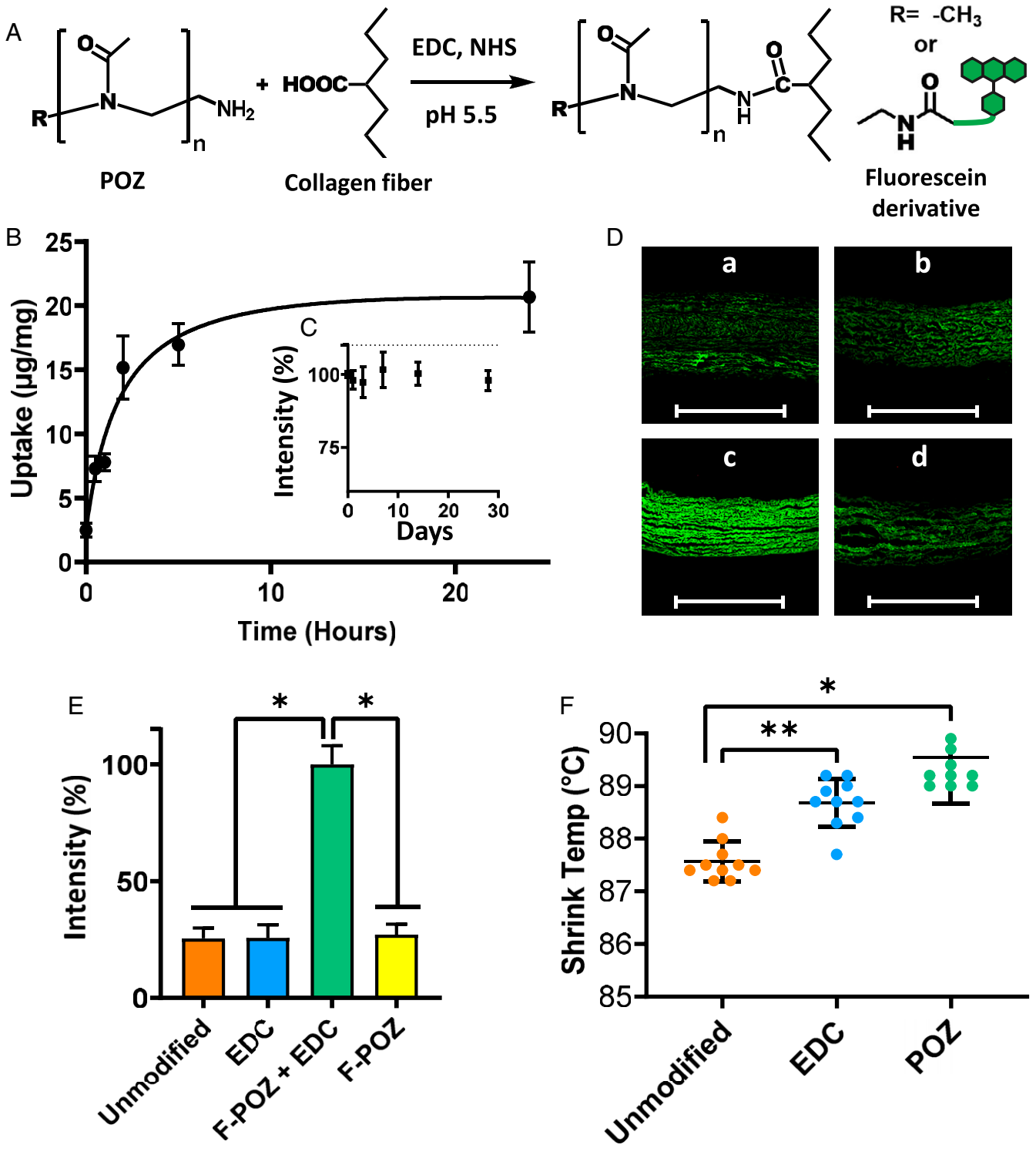

Fig. 2. POZ covalent modification of glutaraldehyde cross-linked BP. (*A*) Schematic of the carbodiimide-driven reaction used to modify BP collagen in bioprosthetic leaflets carboxylic groups with either POZ or F-POZ. Free carboxylic acids are activated with EDC and NHS, forming an NHS ester that reacts with primary amino groups of POZ or fluorescein-POZ conjugate, resulting in amide bond formation. (*B*) POZ conjugation of BP as a function of incubation time. F-POZ was quantitated to determine the extent of POZ incorporation into BP. Error bars indicate SD. (*C*) Stability of F-POZ–labeled BP fluorescent intensity during a 28-d in vitro incubation at physiological conditions in the dark. (*D*) F-POZ reactive uptake and distribution in BP: F-POZ incorporation in frozen sections of BP imbedded in OCT with cross-section images of (*a*) unmodified BP, (*b*) EDC only reacted with BP, (*c*) EDC + F-POZ reacted BP, and (*d*) F-POZ only reacted with BP. (Scale bars, 200 μm.) (*E*) Fluorescent microscopy image intensity analysis: mean relative intensity is plotted on the *y* axis and error bars indicate SD. Images were taken at (λex/λem = 490 nm/515 nm) with 40× magnification. Statistical analyses were performed using one-way ANOVA with Tukey's method (*$P < 0.001$). Only statistically significant differences are indicated. (*F*) Shrink temperature of BP either unmodified (unmodified), or reacted with EDC-NHS (EDC), or modified with POZ (POZ). Error bars indicate SD (*$P < 0.001$, **$P < 0.005$).

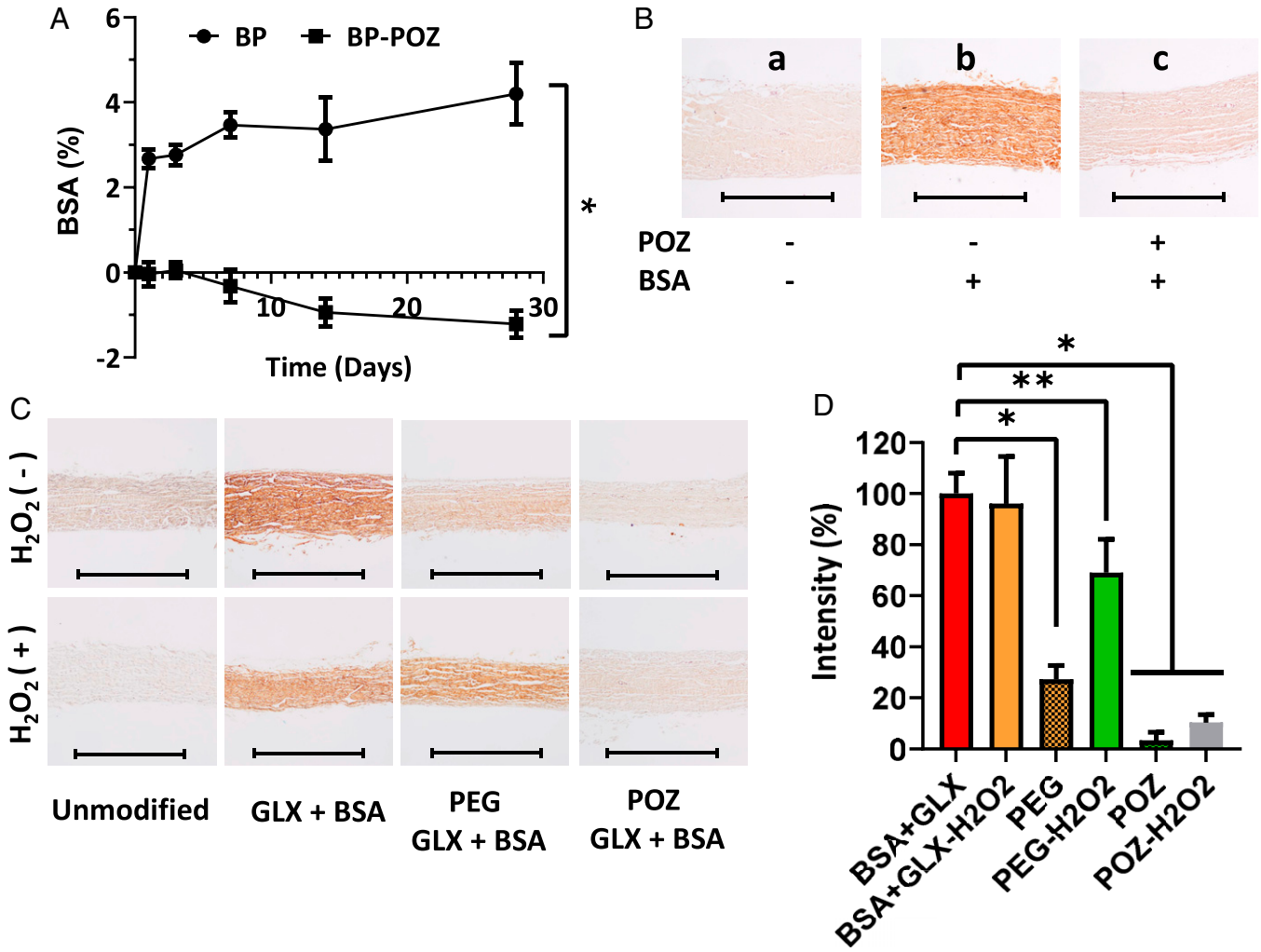

Fig. 3. The effect of POZ on the uptake of BSA by glutaraldehyde cross-linked BP, and CML formation in vitro. BP modified with PEG or POZ compared to nonmodified BP: (*A*) Uptake of BSA expressed as a percentage of the original dry weight of unmodified BP and POZ-modified BP following 28-d incubation with 5% BSA at 37 °C. POZ-modified BP demonstrated significantly less BSA uptake compared to unmodified controls. Error bars indicate SD. Statistical analysis was performed using two-tailed Student's *t* test (*$P < 0.001$). (*B*) IHC staining for αBSA comparing unmodified BP and POZ-modified BP incubated for 28 d in 5% BSA. Images show little detectable staining in BP not exposed to BSA (*a*), compared to intense staining in (*b*) unmodified BP, versus an absence of BSA staining in (*c*) BP-POZ samples. IHC was visualized using HRP-conjugated secondary antibodies and DAB substrate. (Scale bars, 200 μm.) (*C*) IHC staining for CML (αCML) comparing BP modified with 10 kDa PEG or 10 kDa POZ to unmodified BP. Samples were exposed to 10 mM hydrogen peroxide for 7 d followed by incubation in either PBS, GLX alone, or GLX-BSA for 7 d. IHC was visualized using HRP-conjugated secondary antibodies and DAB substrate. (Scale bars, 200 μm.) (*D*) Relative staining intensity using image analysis software (*SI Appendix, Supplementary Methods S1*) of the αCML IHC quantifying the reduction of CML formation following polymeric modification. Unmodified sample was used as 0% intensity; GLX+BSA incubated sample was used as 100% intensity. Error bars indicate SD. Statistical analyses were performed using one-way ANOVA with Tukey's method (*$P < 0.001$, **$P < 0.005$). Only statistically significant differences are indicated.

resulted in a significant increase in TNF-α release per 10^5 cells (Fig. 4*D*, GLU-BSA) ($P < 0.001$). Modification of BP with POZ resulted in a significant reduction of TNF-α levels in GLU-BSA incubated samples ($P < 0.005$) (Fig. 4*D*, BSA). The BP incubation with GLX or GLX+BSA did not induce any significant changes in TNF-α compared to the PBS control (Fig. 4*D*). However, in the GLX+BSA group, BP-POZ was associated with a significant increase in TNF-α production that did not differ significantly from unmodified BP (Fig. 4*D*). This result is consistent with low molecular weight GLX diffusion not being restricted by POZ, thus permeating BP-POZ, thereby resulting in increased TNF-α.

Rat Subdermal Implant Results: BP-POZ and Ethanol Pretreatment Comparisons for Mitigating AGE and Calcification. For rat subdermal implant results (Fig. 5 and *SI Appendix*, Fig. S2), BP and BP-POZ, as well as BP modified with carbodiimide (EDC), as chemistry controls (*Materials and Methods*), were studied in vivo with juvenile rat subdermal implants, a well-established calcification and AGE model (10, 23–25). In addition, separate groups of BP-POZ and BP implants were also pretreated with 100% ethanol, a clinically used BP anticalcification methodology (26). Explanted samples were analyzed by SHG to examine collagen structural changes (Fig. 5*A*). Unimplanted (control) BP had a well-organized collagen structure; however, implantation for 7 d resulted in a disruption of preimplant collagen morphology (Fig. 5*A*). The structure was partially preserved after EDC-NHS modification or ethanol pretreatment alone (Fig. 5*A*, EDC, EtOH). Modification of samples with POZ, with or without ethanol pretreatment, resulted in a stable, organized collagen structure with distinctive bands, similar to unimplanted BP. (Fig. 5*A*, POZ, EtOH+POZ).

Immunostaining of explants using either antiserum albumin or anti-AGE antibody revealed relatively reduced immunostaining for BP-POZ both 7 d (Fig. 5*B*, αAlbumin, αAGE) and 28 d.

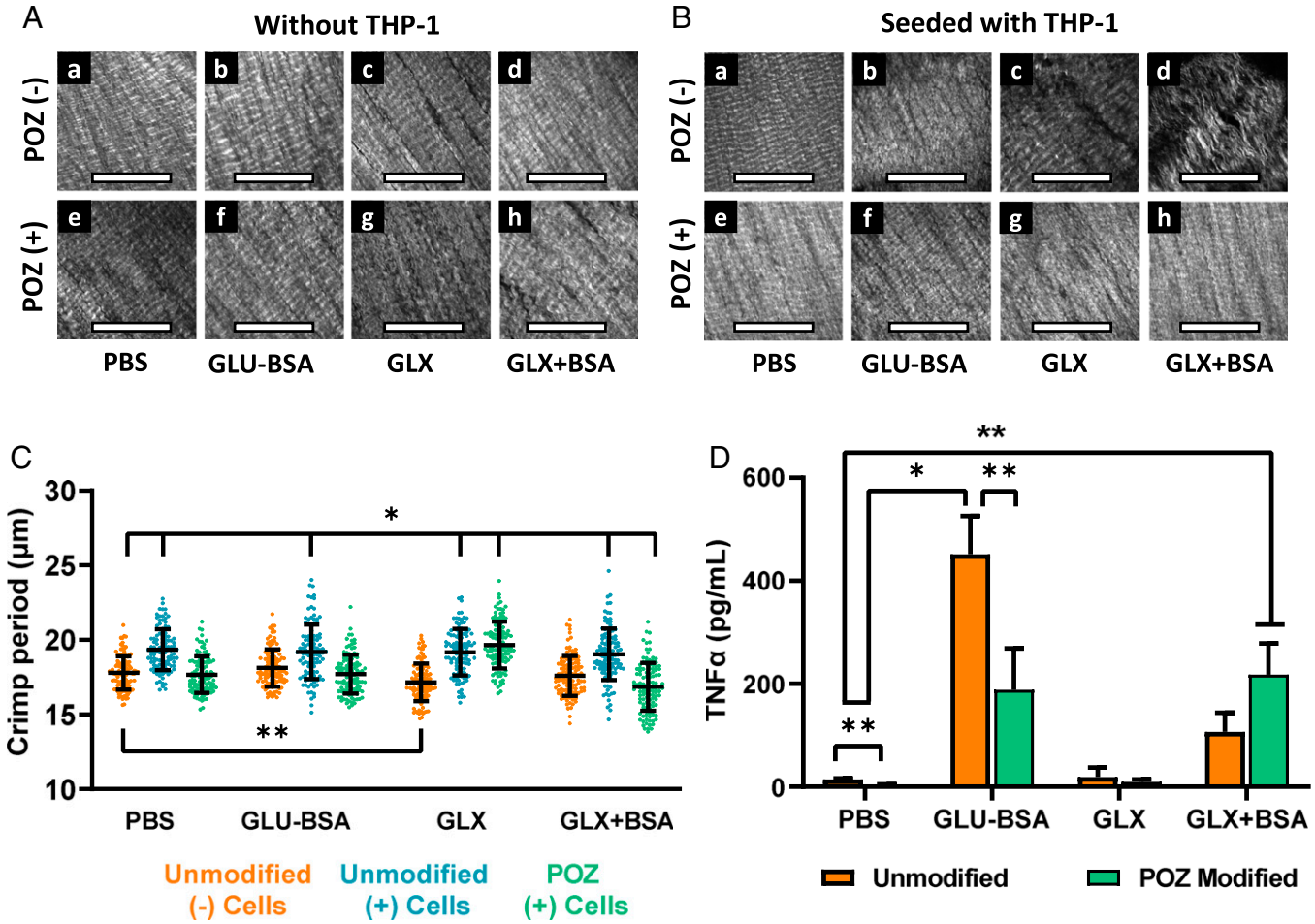

Fig. 4. Comparisons of BP-POZ to BP: The effects of glycation and BSA on collagen structure and inflammatory properties before and after exposure to monocyte-derived macrophages (THP-1). (*A*) Confocal micrographs using SHG imaging of BP-POZ and BP exposed to the following conditions for 7 d: PBS (*a* and *e*), 5% 90-d glucose glycated BSA (GLU-BSA) (*b* and *f*), 50 mM GLX alone (*c* and *g*), or 5% BSA + 50 mM GLX (GLX+BSA) (*d* and *h*) before THP-1 addition. (Scale bars, 100 μm.) (*B*) SHG imaging of BP exposed to the conditions shown after the addition of activated THP-1 macrophages. Following the incubations, BP and BP-POZ samples were rinsed in PBS for 7 d, then used as cell culture substrates for phorbol ester-activated THP-1 cells. BSA and glycation together with THP-1 exposure all showed disruption in collagen structure compared to control samples (*B*, *b–d* vs. *A*, *b–d*). BP-POZ mitigated collagen disruption in GLU-BSA (*f* vs. *b*) and GLX+BSA (*h* vs. *d*). (*C*) Comparison of quantitation of the mean crimp periods (μm) showing significant differences in this structural parameter comparing samples after cell incubation [unmodified (+) cells] to unexposed PBS control [PBS, unmodified (−) cells]. No significant changes were detected in THP-1–exposed groups after BP-POZ [POZ (+) cells], except for GLX. Error bars indicate SD. Significance was determined using Tukey's HSD (*$P < 0.001$, **$P < 0.05$). (*D*) Conditioned media analysis for TNF-α levels (pg/mL per 10^5 cells) after BP exposure to activated THP-1. Following activation, cells were seeded on BP or BP-POZ samples for 48 h, then cell culture media was analyzed for TNF-α levels. Error bars indicate SE. Statistical relationships were analyzed by one-way analysis of variance with Dunnett correction for multiplicity. (*$P < 0.001$, **$P < 0.05$).

The immunostaining for AGE and serum albumin was quantified as a relative color intensity expressed as a percentage using unimplanted BP tissue as 0% and unmodified glutaraldehyde-fixed explant as 100%. There was no significant reduction of the AGE staining intensity in both 7- and 28-d explants after EDC-NHS preincubation (Fig. 5*D*). In contrast, BP-POZ demonstrated a significant reduction of AGE immunostaining intensity for 7- and 28-d explants with 63% and 53%, respectively (Fig. 5*D*). Ethanol preincubation did not significantly affect BP-POZ protection efficiency and AGE immunostaining results for 7-d explants were similar to BP-POZ alone. Staining intensity of 28-d ethanol-treated BP-POZ samples was not significantly reduced compared to unmodified control (Fig. 5*D*).

Immunostaining using an anti-serum albumin antibody revealed albumin uptake in all BP explants after both 7 and 28 d (Fig. 5*B*, αAlbumin). Quantitative image analysis of BP explants preincubated in EDC-NHS showed no significant immunostaining reduction compared to BP-unmodified, with 16% for 7 d and 15% for 28 d (Fig. 5*E*). In contrast, BP-POZ resulted in a significant staining reduction for both 7- and 28-d samples with 49% and 50% reduction, respectively, whereas ethanol pretreatment had a statistically insignificant effect on the IHC staining intensity (Fig. 5*E*).

Von Kossa staining was used for microscopic visualization of calcium deposits in 7- and 28-d explants (Fig. 5*C*, Von Kossa-7d, Von Kossa-28d). Minimal calcium deposits were observed in 7-d samples, while 28-d control, EDC, and POZ developed intense staining. No staining was observed in ethanol-treated groups. Quantitative calcium levels were obtained via acid hydrolysis followed by a colorimetric calcium assay. Calcium analyses of 7-d explants demonstrated complete inhibition of calcification in both of the ethanol-pretreated groups (Fig. 5*F*, 7 d), (EtOH, POZ+EtOH) compared to elevated calcium levels in control, EDC-NHS, and POZ-modified tissues without ethanol pretreatment (Fig. 5*F*, 7 d) (unmodified, EDC, POZ). This anticalcification effect was reduced after 28 d of implantation in both control and POZ-treated tissues showing elevated calcium levels (Fig. 5*F*, 28 d) (EtOH, POZ+EtOH). Calcium

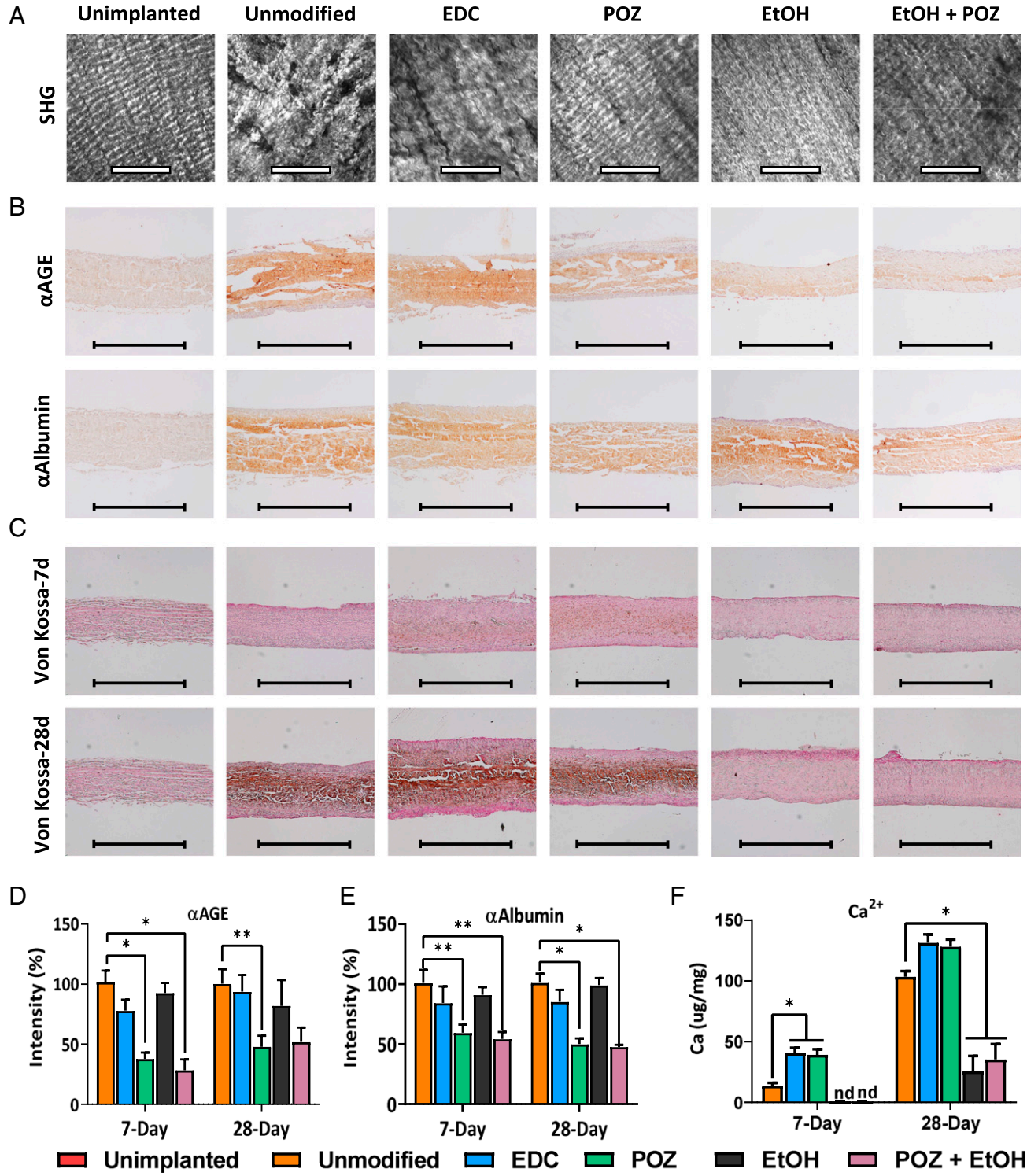

Fig. 5. The effects of POZ modification and ethanol pretreatment on BP collagen structure, AGE formation, serum protein infiltration, and calcification in rat subdermal implants. (*A*) SHG images of 7-d implant collagen structure. All implants were glutaraldehyde-fixed BP (unimplanted) with the following treatments: unmodified, no treatment; EDC, chemistry control incubated in EDC-NHS mixture without POZ; POZ, functionalized with 10 kDa POZ; EtOH, unmodified BP incubated in absolute ethanol for 24 h prior to implantation; EtOH+POZ, POZ-modified BP incubated in absolute ethanol for 24 h prior to implantation. (Scale bars, 100 μm.) (*B*) Implants IHC staining for AGE (αAGE) and serum albumin (αAlbumin). IHC was visualized using HRP-conjugated secondary antibodies and DAB substrate. (Scale bars, 200 μm.) (*C*) Von Kossa calcium specific staining for 7-d explants (Von Kossa-7d) and 28-d explants (Von Kossa-28d) with nuclear fast red as a tissue counterstain. (Scale bars, 200 μm.) (*D*) Relative staining intensity of the αAGE IHC quantifying the reduction of AGE formation following polymeric modification. Unimplanted BP sample was used as 0% intensity, unmodified explants were used as 100% intensity. Error bars indicate SE. For each analysis, *n* of 15 to 20 images was used. (*$P < 0.001$, **$P < 0.05$). (*E*) Relative staining intensity of the α-serum albumin IHC quantifying the reduction of albumin accumulation following polymeric modification. Unimplanted BP sample was used as 0% intensity, unmodified explants were used as 100% intensity. Error bars indicate SE. For each analysis, *n* of 15 to 20 images was used. (*$P < 0.001$, **$P < 0.05$). (*F*) Effects of POZ modification and ethanol pretreatment on calcification: Quantitative calcium results (*Materials and Methods*). Colorimetric calcium level analyses of the explants. Error bars indicate SE (*$P < 0.001$).

analyses of 28 d control, EDC, and POZ-modified explants without ethanol pretreatment showed significantly increased calcium levels in all groups, compared to explants pretreated with ethanol (Fig. 5*F*, 28 d) (unmodified, POZ). No significant differences in shrink denaturation temperature, an index of cross-linking, were recorded using DSC analysis of 7-d unmodified and POZ explants in comparison to controls (*SI Appendix*, Fig. S2*A*), while 28-d samples had a significant decrease ($P < 0.001$) (*SI Appendix*, Fig. S2*B*).

Blood Material Interactions with BP-POZ. In order to study blood material interactions with POZ-modified surfaces (Fig. 6 and *SI Appendix*, Fig. S3), BP-POZ samples were exposed to citrate-anticoagulated whole human blood in comparisons with BP and BP-EDC as controls. These studies were performed using a Chandler loop apparatus, a well-established ex vivo experimental system for investigating blood–material interactions with laminar, high shear flow over surfaces of interest (27). BP samples removed from the Chandler loop after 4 h demonstrated by visual examination (*SI Appendix*, Fig. S2) faint red thrombus on the control BP and BP-EDC samples, but no thrombus on the BP-POZ. SHG studies of these same samples (*SI Appendix*, Fig. S2) confirmed these observations. Scanning electron microscopy (SEM) surface analysis of BP samples after a 4-h Chandler loop study was performed to examine the various BP samples (POZ, EDC, and unmodified) for collagen morphological changes and cellular and thrombotic interactions. SEM analysis with 2,000× magnification of BP samples not exposed to blood (Fig. 6 *A*, *Upper*) revealed comparable surface structures in BP and BP-POZ, while BP-EDC, a chemistry control, had a more irregular surface morphology. Four-hour Chandler loop exposures of the BP samples to citrate-anticoagulated blood demonstrated thrombus formation with platelet, red cell, and white cell deposition on unmodified BP and BP-EDC (Fig. 6 *A*, *Lower*) and minimal platelet deposition with virtually no cellular attachment in the BP-POZ sample (Fig. 6 *A*, *Upper*). Quantitative analyses of SEM images for individual blood components (Fig. 6 *C* and *D*) demonstrated significantly reduced accumulation of red blood cells (RBC), WBCs, and platelets on BP-POZ compared to both unmodified BP and BP reacted with EDC, as a chemistry control (Fig. 6 *C* and *D*) ($P < 0.001$). The SEM results were in agreement with optical and SHG microscopy studies of the same set of samples and experiments (*SI Appendix*, Fig. S3) that demonstrated surface thrombus and RBCs in both BP exposed to blood and BP-EDC. In contrast, BP-POZ demonstrated preserved collagen structure per SHG (*SI Appendix*, Fig. S2), and was comparable to that of unmodified BP not exposed to blood. Thus, POZ modification creates a biocompatible surface that mitigates platelet, RBC, and WBC adhesion on BP while preserving collagen structure.

Discussion

The present study reports biomaterial formulations with POZ-modifications of BP that demonstrated resistance to serum protein infiltration and glycation, modulation of inflammatory events, and enhanced thromboresistance. These findings are of importance for a potential strategy for preventing BHV SVD. Our approach, covalently modifying BP with POZ methodology, has a number of important features: 1) modification of BP, already fixed in glutaraldehyde according to conventional BHV methodology, with POZ was successfully accomplished with stable incorporation of POZ throughout the bulk of the biomaterial; 2) the incorporation of POZ was shown to have no detrimental effects on the BP material properties, such as the shrink temperature, an index of cross-linking, or hydrodynamic parameters, and did not alter BP collagen microstructure; 3) covalently attached POZ significantly mitigated serum protein infiltration and AGE formation in vitro; 4) POZ confers to BP both antiinflammatory and oxidation-resistance properties; 5) POZ mitigates AGE and serum albumin uptake by BP in rat subdermal explants, while not affecting calcification; and 6) POZ modification of BP enhances thromboresistance.

POZ is a biocompatible, nonimmunogenic, and oxidation-resistant polymer that has not previously been studied for its effects on implantable biomaterials. Relevant to this study, POZ has been shown to prevent serum protein adsorption and mitigate cell adhesion to modified glass surfaces (28, 29). Furthermore, POZ covalently attached to BSA significantly reduced the immunogenicity properties of BSA in vivo (30). Importantly, POZ has not been previously investigated in bioprosthetic heart valve formulations.

Several studies have previously evaluated covalently attached PEG for improving the performance and preventing calcification of BHV (31–33). Although reduced calcification was observed after subdermal implantation in rabbits, the mechanical properties of PEGylated implants were compromised, resulting in an increased elastic modulus and tissue swelling (34). Additionally, PEG has been shown to induce an immune response resulting in the formation of anti-PEG antibodies (16). Indeed, numerous studies report the presence of anti-PEG antibodies in human subjects resulting from exposure to PEG and PEGylated products (35). Prior studies have shown vulnerability of PEG to oxidative stress, with a loss of structural integrity and protective effects upon exposure to oxidants (36). It is of importance that in the present study, the integrity and protective capacity of BP-linked POZ was fully retained after exposure to mild oxidative conditions, in contrast to PEG that demonstrated a diminished ability to prevent serum protein adsorption (Fig. 3*C*). Thus, POZ used in formulations with implantable biomaterials may offer a unique combination of excellent biocompatibility, absence of immunogenicity, chemical stability, and resistance to oxidation.

Disruption of collagen microarchitecture is one of the hallmarks of SVD (10, 37). Without covalently attached POZ, all BP samples in the present studies (Figs. 4*B* and 5*A*) showed significant changes in both collagen fiber morphology and collagen crimp period, reflecting a loss of collagen structural integrity following incubation with activated human-derived macrophages exposed to glycated albumin (Fig. 4*B*). In comparison, POZ-modified samples exposed to similar conditions fully retained their uniform collagen structure. The observed disruption of the collagen structure in vivo is likely the result of both AGE and serum protein infiltration and oxidative damage caused by activated macrophages as part of the inflammatory response (7). Furthermore, POZ modification of BP compared to unmodified BP resulted in significantly reduced TNF-α secretion in THP-1 cell cultures (Fig. 4*D*) with BP pre-exposed to BSA or glucose-glycated BSA, thus demonstrating an antiinflammatory effect.

Along with serum protein and AGE accumulation, calcification is another major contributor to BHV failure. The pathophysiology of BHV calcification involves initial mineral deposits in the glutaraldehyde-devitalized cells of the central spongiosa region of BHV leaflets followed by calcification of the collagen rich extracellular matrix (24, 38). Importantly, BHV do not become endothelialized, nor are they populated by viable valvular interstitial cells (24, 38); this lack of a viable cellular component makes BHV leaflets particularly vulnerable to protein glycation and serum protein infiltration pathophysiology. We used a well-established rat subdermal model of BHV SVD (24), which results in BHV calcification pathology that has been demonstrated to be comparable to clinical circulatory BHV explants (24); this rat subdermal model also replicates clinically observed stress localized calcification in folded leaflet regions (38). Recent

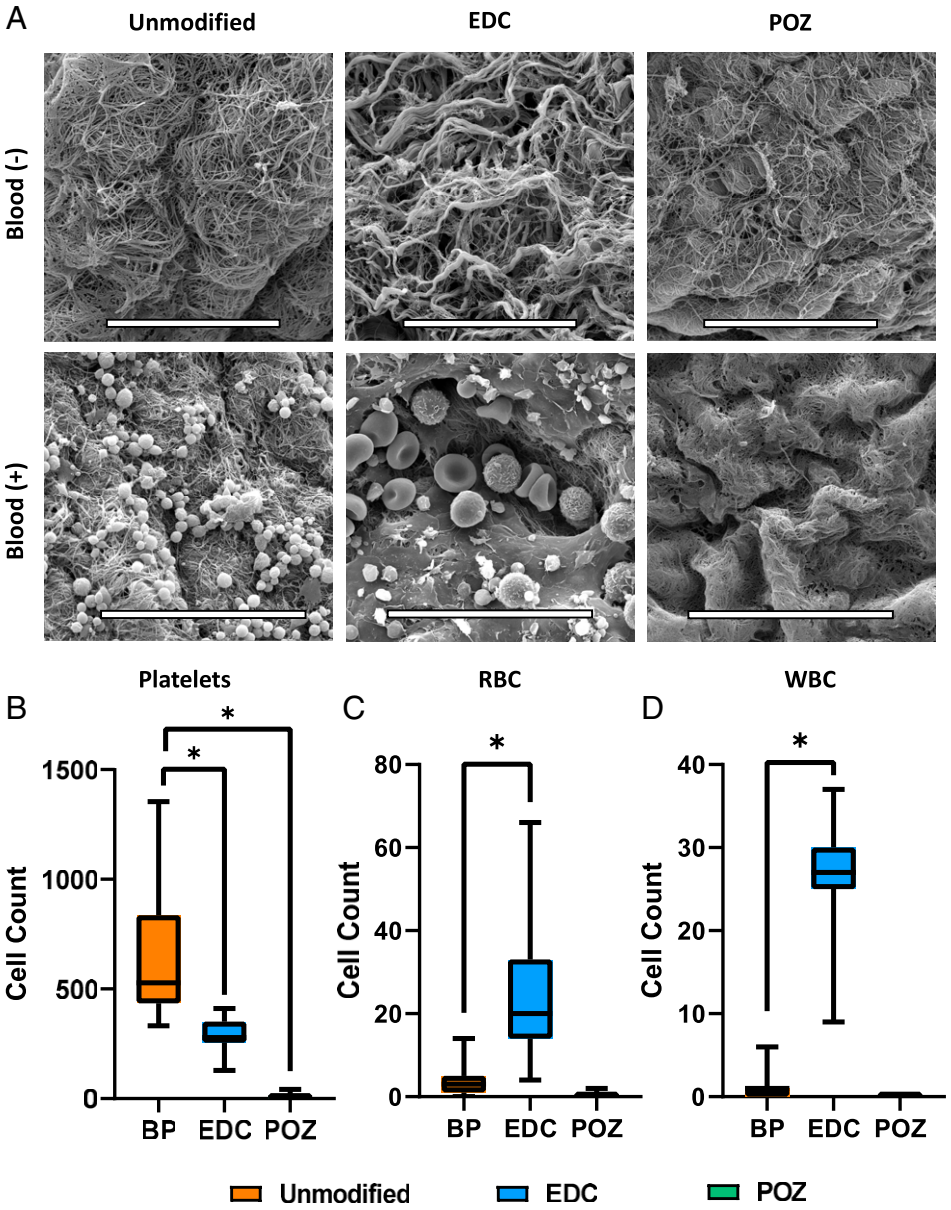

Fig. 6. Representative SEM images to show the effects of POZ modification on BP collagen surface and blood-material interactions examined with SEM. (*A*) SEM micrograph of unmodified BP, after EDC-NHS incubation, after POZ modification prior to blood exposure (*Upper*) and after citrated whole human blood exposure for 4 h (*Lower*). (Scale bars, 30 μm.) Quantitative analyses adherent blood cells for platelets (*B*), RBCs (*C*) and WBCs (*D*) measured by analysis of SEM images. A minimum of 12 fields were analyzed for each condition. Error bars indicate SD. Statistical analyses were performed using Dunnett's test (*$P < 0.001$).

studies by our group have also demonstrated comparable AGE-serum protein deposition in rat subdermal explants and retrieved clinical BHV with SVD, thus validating the rat subdermal model for investigating AGE-serum protein pathophysiology (10, 25). The present subdermal studies concomitantly evaluated both serum protein and AGE accumulation in BP, and calcification of glutaraldehyde-fixed BP with or without POZ modification. These studies tested the hypothesis that these represent two independent phenomena driven by separate mechanisms. Unmodified BP subdermal implants in rats, when explanted, all showed significant serum protein uptake, AGE accumulation, collagen disruption, and calcification (Fig. 5). These data are in agreement with our previous in vitro study, showing that serum protein uptake and glycation along with mechanical stress results in BP collagen disruption (19). In comparison, POZ modification significantly reduced serum protein uptake, AGE accumulation, and collagen disruption, but had no effect on calcification, consistent with distinct mechanisms responsible for glycation and calcification.

Importantly, BP preincubation with ethanol prior to implantation significantly reduced calcification (Fig. 5), as expected based on prior studies (39), while not affecting AGE and serum albumin uptake levels. However, when combined with POZ modification, ethanol pretreatment of BP also resulted in a significant reduction in explant Ca levels and negative Von Kossa staining (Fig. 5), supporting the view that these two distinct mechanisms driving BHV failure, calcification, and AGE-serum protein uptake, can be addressed effectively yet separately. Thus, a combination of POZ attachment to BP and ethanol pretreatment may potentially be applied as an approach for protecting BHV from deterioration due to both glycation and calcification.

The results of the Chandler loop experiments demonstrated thromboresistance of BP-POZ, compared to the control BP

samples (Fig. 6). It should be noted that BHV fabricated from BP and other heterograft materials are considered to be relatively thromboresistant (40). Nevertheless, under the experimental conditions studied with citrate anticoagulated human blood, a finite fibrin surface thrombus with associated cellular and platelet deposition was demonstrated with control BP samples (Fig. 6), but not BP-POZ. In addition, although serum protein permeation of BP is mitigated by POZ modification (Fig. 3), the well-known passivation of blood contacting material surfaces by serum proteins contributing to thromboresistance (41) would not be expected to be altered by POZ; the Chandler loop results (Fig. 6) support this view. In addition, these results are of importance since prior to these studies the blood material compatibility and thromboresistance of POZ had not been explored, and thus needed to be established. Taken together, these results show that POZ modification of BP results in enhanced thromboresistance.

Orthotopic or transcatheter bioprosthetic heart valve replacements in large animals, typically sheep (42), would be requisite preclinical studies for POZ-modified BHV to move ahead for consideration for regulatory approval. Nevertheless, large animal BHV studies are carried out for durations of only 5 to 6 mo (42), as required by regulatory agencies, and because of this limitation heart valve replacement studies in large animals have provided little mechanistic information about SVD. Therefore, the lack of large animal investigations in the present studies of the mechanistic effects of POZ modifications does not represent a significant limitation that impacts the results. Another limitation of the present studies involves the results included in *SI Appendix*, Fig. S4 and Tables S1–S5, which were concerned with POZ effects on trileaflet BHV hydrodynamics, utilizing five clinical-grade BHVs. The prohibitive cost of clinical grade trileaflet BHV, and the highly variable baseline hydrodynamics of trileaflet BHV, even of the same size (43), are major limitations for carrying out this type of experiment. The effects of POZ-modification mitigating the effects of protein glycation on the hydrodynamic function of these trileaflet BHV, while statistically significant (*SI Appendix*, *Supplementary Results S1* and Fig. S4), were not clinically relevant. Another limitation of these hydrodynamic studies are the small changes in the PBS baseline for the pressure gradient and peak ejection-velocity parameters that changed in parallel with the other results under glycation conditions (*SI Appendix*, Fig. S4 and Tables S1 and S2). The reasons for the changes in PBS-incubated BHV are difficult to determine, but may be related to PBS storage over the 35-d time course, since bioprosthetic valves are typically stored in glutaraldehyde, and glutaraldehyde has been shown to dissociate over time from bioprosthetic leaflets in vivo (44) and from histology specimens stored in physiologic buffers (45), thereby hypothetically changing mechanical properties. Nevertheless, baseline testing of trileaflet BHV before and after POZ modification (*SI Appendix*, Tables S2 and S5) demonstrated that POZ modification does not significantly alter the initial hydrodynamics, indicating that leaflet mechanical properties are not negatively impacted by POZ.

The thromboresistance and antiinflammatory properties of BP-POZ demonstrated in the present studies (Figs. 4 and 6) indicate that POZ modification of other biomaterials merits further investigation. POZ has been used in plasma-mediated material coatings (46), and thus could hypothetically be broadly applied for medical device use to mitigate thrombosis and enhance biocompatibility. Furthermore, our results showed that POZ can be efficaciously combined with an established anticalcification strategy (Fig. 5), ethanol pretreatment of BHV, currently in clinical use (47). Thus, the results of these investigations could be the basis for a novel approach, combining anticalcification and AGE-serum protein mitigation strategies, for the next generation of BHV, ultimately improving the durability of these widely used devices and addressing a major unmet need.

In conclusion, our studies demonstrated that BP modification with POZ has the potential to mitigate protein-glycation SVD mechanisms, and markedly improve biocompatibility, as demonstrated in the results of these studies showing enhanced thromboresistance, a reduced inflammatory response, and oxidation resistance.

Materials and Methods

Materials. Mono- and diamino-functionalized POZ, (10 kDa) were chosen as optimized polymers; these compounds were purchased from Ultroxa. 5(6)-carboxyfluorescein *N*-hydroxysuccinimide ester (≥80%) was purchased from Sigma. Antibodies were purchased from Abcam: anti-BSA antibody (ab192603), anti-AGE antibody (ab23722), anti-CML antibody (ab125145). Glutaraldehyde was purchased from Polysciences. Biosol was purchased from National Diagnostics. Pharmaceutical grade human serum albumin (HSA), used in the clinical grade trileaflet BHV experiments, was purchased from Octapharma. THP-1 cells, a monocyte/macrophage cell line, were purchased from ATCC. RPMI medium was purchased from Cell Culture Technologies. TNF-α ELISA was obtained from Invitrogen. Cellulose dialysis membrane was purchased from Spectrum Labs (10768-700). The Von Kossa staining kit was obtained from Abcam (ab150687). All chemicals were purchased from Sigma Aldrich, unless otherwise stated.

BP Preparation. BP was purchased in a fresh state, and was transported within 24 h, on ice from Animal Technologies. Fresh BP was treated with 0.625% glutaraldehyde in Hepes buffer (50 mM Hepes, 0.9% NaCl, pH 7.4) for 7 d at room temperature. BP was transferred into 0.2% glutaraldehyde Hepes solution and stored at 4 °C. Shrink temperature methods as a metric of cross-linking using DSC are described in *SI Appendix, Supplementary Methods S1*.

POZ Modification. For POZ attachment, BP functionalization through covalent modification of carboxylic groups with POZ via a carbodiimide-driven reaction. was carried out as follows: BP samples (1 × 1 cm) were rinsed three times with PBS solution and placed in 1 mL of MES buffer (pH 5.5) solution with 10 mg of POZ overnight at 37 °C. To initiate the reaction, 43 mM NHS and 65 mM of EDC were added in 1 mL MES to a total volume of 2 mL. The reaction proceeded for 24 h at room temperature with mild shaking. Fluorescent POZ synthesis and methodology are described in detail in *SI Appendix, Supplementary Methods S1*)

Protein Glycation Procedures. GLU-BSA was obtained by incubating 5% (wt/wt) BSA in PBS buffer (pH 7.4) with 100 mM glucose in vitro for 90 d at 37 °C in the dark. After the reaction, glycated BSA was dialyzed using a cellulose ester membrane (Spectra Por 131342T) with a 20-kDa cutoff against PBS to remove unbound glucose, before lyophilization, and storage at −20 °C in the dark. Modification of GLX+BSA was carried out in vitro by reacting BSA (5%) (wt/vol) with 50 mM GLX for 7 d at 37 °C in the dark. For accelerated glycation of BP, glutaraldehyde-fixed BP samples were created using 8-mm biopsy punches and incubated for 7 d in PBS, 5% BSA, GLU-BSA, GLX+BSA, or 50 mM GLX, then rinsed for 7 d in sterile PBS for to remove unbound AGE and excess glutaraldehyde. Trileaflet clinical grade BHV were also studied with this same methodology (*SI Appendix, Supplementary Methods S1*). Immunostaining techniques and immunostaining quantitation methods to detect serum albumin and AGE are described in *SI Appendix, Supplementary Methods S1*.

Cell Culture Methods. The human monocyte cells (THP-1 line) were cultured in RPMI medium (Sigma Aldrich R8758) supplemented with 10% fetal bovine serum and 1% penicillin-streptomycin. Monocytes were differentiated to monocyte derived macrophages using 100 ng/mL PMA and seeded on BP surfaces using the same medium composition. Cell culture was maintained in a 37 °C incubator with 5% CO_2 under a humidified atmosphere. Experiments were conducted at a cell concentration of 2×10^5 cells/mL BP discs (8 mm in diameter), with or without glycation, were used as substrates for THP-1 cells. Discs were placed in 48-well culture plates with a pericardial side facing up and cells were seeded in PMA media. After 24 h of incubation with cells, the medium was collected to measure TNF-α using an ELISA according to manufacturer's instructions by measuring the optical density at 450 nm.

SHG Microscopy. To image collagen structure morphology, round BP samples (8 mm in diameter) were mounted on incubation chambers (Electron Microscopy Sciences) and immersed in PBS between two glass coverslips. SHG images were acquired with Prairie Technologies Ultima multiphoton system attached to an Olympus BX-61 upright microscope. Excitation light was provided by a

diode-pumped broadband mode-locked titanium: sapphire femtosecond Mai-Tai HP laser (Spectra Physics). The laser beam was focused on the sample by a 20× water-immersion objective (Olympus xlumplfln). The excitation wavelength of 920 nm with a 505-nm short-pass filter optimal for collagen imaging was used as previously reported (48). SHG image analysis methodology is described in *SI Appendix, Supplementary Methods S1*.

Rat Subdermal BP Implants. Male juvenile (3 wk of age, average weight of 75 g) Sprague-Dawley rats (Charles-River Laboratories) received subdermal BP implants under general anesthesia (isoflurane), as previously published (24). All protocols were approved by the Institutional Committee for the Use and Care of Animals of The Children's Hospital of Philadelphia. The BP implants were 10×10 mm^2 glutaraldehyde-fixed BP patches with the following modifications: 1) unmodified; 2) ethanol-pretreated (24 h, room temperature); 3) POZ-modified; 4) ethanol-treated and POZ-modified. Each animal was implanted with one implant from each group, in cohorts of 10 rats per time point. Animals were killed at 7 and 28 d after implantation and harvested explants were rinsed in sterile saline. Half of each explant was either frozen or placed in 10% neutral buffered formalin for histological processing.

Rat Subdermal BP Explants Calcium Analysis. For the calcium analysis, samples were lyophilized, weighed, and hydrolyzed with 6M hydrochloric acid. Calcium content was determined using a colorimetric assay (Sigma MAK022).

Chandler Loop Apparatus Experiments. Samples of BP, BP-EDC, or BP-POZ were secured inside the closed polyvinylchloride tube (Terumo Cardiovascular Systems) system. Ten milliliters of citrated whole blood from healthy human volunteers, as approved by the Children's Hospital of Philadelphia Protocol IRB #008608, was perfused through the tubing for 4 h at a calculated shear force of 25 dynes/cm^2 (27). At the end of 4 h, the blood was drained from the tubes and the BP inserts were retrieved. Next, samples were gently rinsed with saline, fixed with 0.6% glutaraldehyde prior to examination with optical microscopy, SHG, and SEM. SEM methods are described in *SI Appendix, Supplementary Methods S1*.

Statistical Methods. Statistical analyses of microscopic images' intensity were performed using one-way ANOVA and treatments were compared to control for multiplicity using Tukey honestly significant difference (HSD). The significance of the effects of POZ modification on BSA mass uptake was determined by two-tailed Student's *t* test. For each sample, the significance of dry mass change was evaluated in comparison with initial mass prior to incubation. For crimp period analysis to determine the significance of the changes in crimp period for each incubation to the PBS control, Dunnett's test was used to control for multiplicity. TNF-α statistical relationships were analyzed by one-way ANOVA with Dunnett correction for multiplicity. Pulse duplicator statistical analyses were performed using two-way ANOVA. Bonferroni-adjusted *P* values were used (since there were three tests, each original value was multiplied by three) to control for multiplicity. For all statistical tests, $P < 0.05$ was considered significant. In one-way analysis, if all levels are compared then Tukey's HSD was used to adjust for multiplicity. In one-way analysis when each treatment was compared to a control, the *P* value was adjusted for multiplicity using Dunnett's method. In the two-way ANOVA, since three comparisons are made, to be conservative, the Bonferroni-adjusted *P* values were used (i.e., each original *P* value was multiplied by three). For all statistics tests, $P < 0.05$ was considered significant. In cases where there might be concern that the data are skewed and hence *P* values using conventional normal theory might be suspect, we also performed nonparametric tests: where the two-sample *t* tests was performed, a Wilcoxon rank sum test was run; where a one-way ANOVA was performed, a Kruskal–Wallis test was run. The resulting *P* values for the nonparametric tests were substantively the same.

Data Availability. All study data are included in the main text and supporting information.

ACKNOWLEDGMENTS. We thank Susan Kerns for manuscript preparation and submission, and Emily Hall for help with differential scanning calorimetry measurements and sample preparation. This work was supported by the following: NIH Grants HL143008 (to G.F. and R.J.L.) and HL007915 (to A.Z., C.A.R., and R.J.L.); the Congenital Heart Defect Coalition (A.Z.); The Pediatric Heart Valve Center of the Children's Hospital of Philadelphia (R.J.L.); The Kibel Fund for Aortic Valve Research (G.F. and R.J.L.); The Valley Hospital Foundation "Marjorie C Bunnel" charitable fund (G.F.); the Andrew Sabin Family Foundation Research Laboratory (G.F.); and both the Erin's Fund and the William J. Rashkind Endowment of the Children's Hospital of Philadelphia (R.J.L.).

1. C. M. Otto *et al.*, 2020 ACC/AHA guideline for the management of patients with valvular heart disease: A report of the American College of Cardiology/American Heart Association Joint Committee on Clinical Practice Guidelines. *Circulation* **143**, e72–e227 (2021).
2. P. Pibarot, J. G. Dumesnil, Prosthetic heart valves: Selection of the optimal prosthesis and long-term management. *Circulation* **119**, 1034–1048 (2009).
3. R. F. Siddiqui, J. R. Abraham, J. Butany, Bioprosthetic heart valves: Modes of failure. *Histopathology* **55**, 135–144 (2009).
4. E. L. Johnson *et al.*, Thinner biological tissues induce leaflet flutter in aortic heart valve replacements. *Proc. Natl. Acad. Sci. U.S.A.* **117**, 19007–19016 (2020).
5. D. Dvir *et al.*; VIVID (Valve in Valve International Data) Investigators, Standardized definition of structural valve degeneration for surgical and transcatheter bioprosthetic aortic valves. *Circulation* **137**, 388–399 (2018).
6. L. Søndergaard *et al.*, Durability of transcatheter and surgical bioprosthetic aortic valves in patients at lower surgical risk. *J. Am. Coll. Cardiol.* **73**, 546–553 (2019).
7. A. E. Kostyunin *et al.*, Degeneration of bioprosthetic heart valves: Update 2020. *J. Am. Heart Assoc.* **9**, e018506 (2020).
8. S. Lee *et al.*, Calcification and oxidative modifications are associated with progressive bioprosthetic heart valve dysfunction. *J. Am. Heart Assoc.* **6**, e005648 (2017).
9. M. Marro *et al.*, Noncalcific mechanisms of bioprosthetic structural valve degeneration. *J. Am. Heart Assoc.* **10**, e018921 (2021).
10. A. Frasca *et al.*, Glycation and serum albumin infiltration contribute to the structural degeneration of bioprosthetic heart valves. *JACC Basic Transl. Sci.* **5**, 755–766 (2020).
11. R. W. Moreadith *et al.*, Clinical development of a poly(2-oxazoline) (POZ) polymer therapeutic for the treatment of Parkinson's disease—Proof of concept of POZ as a versatile polymer platform for drug development in multiple therapeutic indications. *Eur. Polym. J.* **88**, 524–552 (2017).
12. A. W. Bridges, A. J. García, Anti-inflammatory polymeric coatings for implantable biomaterials and devices. *J. Diabetes Sci. Technol.* **2**, 984–994 (2008).
13. A. J. T. Teo *et al.*, Polymeric biomaterials for medical implants and devices. *ACS Biomater. Sci. Eng.* **2**, 454–472 (2016).
14. S. Aravind, W. Paul, S. C. Vasudev, C. P. Sharma, Polyethylene glycol (PEG) modified bovine pericardium as a biomaterial: A comparative study on immunogenicity. *J. Biomater. Appl.* **13**, 158–165 (1998).
15. S. Sharma, R. W. Johnson, T. A. Desai, Evaluation of the stability of nonfouling ultrathin poly(ethylene glycol) films for silicon-based microdevices. *Langmuir* **20**, 348–356 (2004).
16. B. Reid *et al.*, PEG hydrogel degradation and the role of the surrounding tissue environment. *J. Tissue Eng. Regen. Med.* **9**, 315–318 (2015).
17. Q. Yang *et al.*, Analysis of pre-existing IgG and IgM antibodies against polyethylene glycol (PEG) in the general population. *Anal. Chem.* **88**, 11804–11812 (2016).
18. A. J. Christian *et al.*, The susceptibility of bioprosthetic heart valve leaflets to oxidation. *Biomaterials* **35**, 2097–2102 (2014).
19. C. A. Rock *et al.*, Model studies of advanced glycation end product modification of heterograft biomaterials: The effects of in vitro glucose, glyoxal, and serum albumin on collagen structure and mechanical properties. *Acta Biomater.* **123**, 275–285 (2021).
20. A. Simionescu, D. T. Simionescu, R. F. P. Deac, Matrix metalloproteinases in the pathology of natural and bioprosthetic cardiac valves. *Cardiovasc. Pathol.* **5**, 323–332 (1996).
21. S. Reddy, J. Bichler, K. J. Wells-Knecht, S. R. Thorpe, J. W. Baynes, N epsilon-(carboxymethyl)lysine is a dominant advanced glycation end product (AGE) antigen in tissue proteins. *Biochemistry* **34**, 10872–10878 (1995).
22. A. Schmitt, J. Schmitt, G. Münch, J. Gasic-Milencovic, Characterization of advanced glycation end products for biochemical studies: Side chain modifications and fluorescence characteristics. *Anal. Biochem.* **338**, 201–215 (2005).
23. J. M. Connolly *et al.*, Triglycidyl amine crosslinking combined with ethanol inhibits bioprosthetic heart valve calcification. *Ann. Thorac. Surg.* **92**, 858–865 (2011).
24. F. J. Schoen *et al.*, Onset and progression of experimental bioprosthetic heart valve calcification. *Lab. Invest.* **52**, 523–532 (1985).
25. Y. Xue *et al.*, Age-related enhanced degeneration of bioprosthetic valves due to leaflet calcification, tissue crosslinking, and structural changes. *Cardiovasc. Res.*, 10.1093/cvr/cvac002 (2021).
26. N. R. Vyavahare, P. L. Jones, D. Hirsch, F. J. Schoen, R. J. Levy, Prevention of glutaraldehyde-fixed bioprosthetic heart valve calcification by alcohol pretreatment: Further mechanistic studies. *J. Heart Valve Dis.* **9**, 561–566 (2000).
27. J. B. Slee, I. S. Alferiev, R. J. Levy, S. J. Stachelek, The use of the ex vivo Chandler Loop Apparatus to assess the biocompatibility of modified polymeric blood conduits. *J. Vis. Exp.* **90**, 51871 (2014).
28. N. Zhang *et al.*, Tailored poly(2-oxazoline) polymer brushes to control protein adsorption and cell adhesion. *Macromol. Biosci.* **12**, 926–936 (2012).
29. T. Lorson *et al.*, Poly(2-oxazoline)s based biomaterials: A comprehensive and critical update. *Biomaterials* **178**, 204–280 (2018).
30. T. X. Viegas *et al.*, Polyoxazoline: Chemistry, properties, and applications in drug delivery. *Bioconjug. Chem.* **22**, 976–986 (2011).
31. S. C. Vasudev, T. Chandy, C. P. Sharma, The antithrombotic versus calcium antagonistic effects of polyethylene glycol grafted bovine pericardium. *J. Biomater. Appl.* **14**, 48–66 (1999).
32. K. D. Park *et al.*, Novel anti-calcification treatment of biological tissues by grafting of sulphonated poly(ethylene oxide). *Biomaterials* **18**, 47–51 (1997).
33. M. A. Roseen *et al.*, Poly(ethylene glycol)-based coatings for bioprosthetic valve tissues: Toward restoration of physiological behavior. *ACS Appl. Bio Mater.* **3**, 8352–8360 (2020).

34. A. Carpentier, A. Nashef, S. Carpentier, A. Ahmed, N. Goussef, Techniques for prevention of calcification of valvular bioprostheses. *Circulation* **70**, I165–I168 (1984).
35. J. K. Armstrong *et al.*, Antibody against poly(ethylene glycol) adversely affects PEG-asparaginase therapy in acute lymphoblastic leukemia patients. *Cancer* **110**, 103–111 (2007).
36. B. Pidhatika *et al.*, Comparative stability studies of poly(2-methyl-2-oxazoline) and poly(ethylene glycol) brush coatings. *Biointerphases* **7**, 1 (2012).
37. S. L. Sellers, P. Blanke, J. A. Leipsic, Bioprosthetic heart valve degeneration and dysfunction: Focus on mechanisms and multidisciplinary imaging considerations. *Radiol. Cardiothorac. Imaging* **1**, e190004 (2019).
38. F. J. Schoen, R. J. Levy, Founder's Award, 25th Annual Meeting of the Society for Biomaterials, perspectives. Providence, RI, April 28–May 2, 1999. Tissue heart valves: Current challenges and future research perspectives. *J. Biomed. Mater. Res.* **47**, 439–465 (1999).
39. N. Vyavahare *et al.*, Prevention of bioprosthetic heart valve calcification by ethanol preincubation. Efficacy and mechanisms. *Circulation* **95**, 479–488 (1997).
40. F. J. Schoen, R. J. Levy, Pathology of substitute heart valves: New concepts and developments. *J. Card. Surg.* **9** (2, suppl.), 222–227 (1994).
41. J. N. Mulvihill, A. Faradji, F. Oberling, J. P. Cazenave, Surface passivation by human albumin of plasmapheresis circuits reduces platelet accumulation and thrombus formation. Experimental and clinical studies. *J. Biomed. Mater. Res.* **24**, 155–163 (1990).
42. F. J. Schoen, D. Hirsch, R. W. Bianco, R. J. Levy, Onset and progression of calcification in porcine aortic bioprosthetic valves implanted as orthotopic mitral valve replacements in juvenile sheep. *J. Thorac. Cardiovasc. Surg.* **108**, 880–887 (1994).
43. S. Marquez, R. T. Hon, A. P. Yoganathan, Comparative hydrodynamic evaluation of bioprosthetic heart valves. *J. Heart Valve Dis.* **10**, 802–811 (2001).
44. C. L. Webb, F. J. Schoen, R. J. Levy, Covalent binding of aminopropanehydroxydiphosphonate to glutaraldehyde residues in pericardial bioprosthetic tissue: Stability and calcification inhibition studies. *Exp. Mol. Pathol.* **50**, 291–302 (1989).
45. K. G. Helander, S. Widéhn, H. F. Helander, Kinetic studies of glutaraldehyde binding in liver. *Biotech. Histochem.* **77**, 207–212 (2002).
46. M. N. Ramiasa *et al.*, Plasma polymerised polyoxazoline thin films for biomedical applications. *Chem. Commun. (Camb.)* **51**, 4279–4282 (2015).
47. G. Mariscalco *et al.*, St. Jude Medical Trifecta aortic valve: Results from a prospective regional multicentre registry. *J. Cardiothorac. Surg.* **10**, 169 (2015).
48. N. H. Green *et al.*, A new mode of contrast in biological second harmonic generation microscopy. *Sci. Rep.* **7**, 13331 (2017).